Wesleyan University

Decisive Solution to a Long-standing Controversy in Paul-Trap Physics

by

Chi Hang Kan

Class of 2017

An honors thesis submitted to the

faculty of Wesleyan University

in partial fulfillment of the requirements for the

Degree of Bachelor of Arts

with Departmental Honors in Physics

Middletown, Connecticut May, 2017

Abstract

The study of charged particles' dynamics in a Paul trap is the foundation of its wide-ranging applications, including analyzing proteins, determining isotope ratios, and constructing a quantum computer. However, in the simplest case of two-particle dynamics, there remains a controversy on whether a two-ion planar crystal undergoes an order→chaos transition at a critical trap parameter value. Via linearization and separation of the *Mathieu-Coulomb* equations, this thesis shows analytically and numerically that the transition does not exist. Furthermore, the method developed here can be extended to determine the stability and existence of two-ion crystals in the whole parameter space of both the hyperbolic and linear Paul trap.

Dedication

To my family.

Acknowledgments

I would like to acknowledge my research advisor, Professor Reinhold Blümel, and research collaborator, Dr. Yunseong Nam, for their guidance throughout my time in this group. I would also like to thank my fellow group members, Danny Weiss and Varun Ursekar, for making my summer research experience more fun and less lonely.

Contents

List of Figures

Chapter 1

Introduction

1.1 Motivations and Applications

In natural science, the ability to observe and measure microscopic interactions is of utmost importance because of two major reasons. First, natural science is based on empirical evidence. Second, in order to understand complex natural phenomena, modern scientists adopt the reductionist approach. They reduce complicated observations into smaller parts and try to comprehend the fundamental interactions between them. Then, they piece them back together to see the larger picture. That is why the invention of apparatuses, such as microscopes and telescopes, is considered revolutionary.

For the same reasons, the invention of the Paul Trap was deemed groundbreaking, so much so that the inventor, Wolfgang Paul, was awarded the Nobel Prize in Physics. The Paul Trap is a device designed to suspend particles using only dynamic electric fields, instead of material walls [1]. Its applications in physics include exploring nonlinear dynamics [2], realizing a discrete time crystal [3],

and constructing a quantum computer [4]. In fact, its contribution to science extends beyond physics. Both chemists and biologists widely utilize it as a mass spectrometer [5] to determine isotope ratios [5], analyze proteins [6], etc. It may even have biomolecular and medicinal applications as the Paul Trap was shown experimentally to be capable of confining charged particles in aqueous solution [7], and numerical studies demonstrated that it could even trap a DNA segment [8].

As wide-ranging as the Paul Trap's applications are, the basis of all its applications rests on the dynamics of trapped charged particles. This thesis contributes to the Paul Trap community by solving a controversy in the dynamics of trapped charged particles.

1.2 The Controversy: Stability of Coulomb Crystals in a Paul Trap

The Paul Trap captures charged particles by applying an ac voltage, often combined with a dc voltage, to the hyperbolic electrodes. Due to the oscillating electric field inside the trap, generated by the applied voltages to the electrodes, a focussing force, emergent when averaged over many oscillation cycles, is exerted on a particle in the trap. This force, using the amplitude and frequency of the field, may be tuned convergent to or divergent from the center of the trap. This then leads to confinement or escape of the particle, respectively.

The exact combinations of ac and dc voltages that lead to stable trapping of an ion can be mathematically determined. The diagram that maps out such combinations is denoted as the Mathieu stability diagram.

With more than one ion in a Paul Trap, chaos may emerge because of the nonlinear Coulomb interaction. However, it is entirely possible to produce an ordered dynamics, i.e., crystals, where the phase-space vector of the trapped ions undergoes periodic motion, in phase with the trap drive, and hence, appears stroboscopically constant. Moreover, once the trapped ions crystallize, they do not heat [9] and hence, remain a crystal, the least energetic state.

In order for the ions to settle into a crystalline state, they need to first satisfy two stability criteria. First, the ions need to be stably trapped. In other words, the center-of-mass motion needs to remain near the center of the trap. Second, the trapped ions' relative motion need to remain bounded, and thus does not increase exponentially, so as for the ions not to hit the electrodes or to escape from the trap.

Indeed, the Mathieu stability diagram gives us an excellent idea of the ions' center-of-mass stability, since the Coulomb interaction is irrelevant for determining the center-of-mass stability. However, in order to form a crystal, the position and velocity of the ions are required to be stroboscopically constant. Hence, we also need the relative motion of the ions to be stable. It is important to recognize that the Mathieu stability does not imply relative-motion stability, and vice versa. Indeed, there are *crystal-free* regions in the Mathieu stability diagram, where the stably trapped ions' relative motion is unstable [10], and hence, they cannot settle into a crystalline state. Furthermore, the addition of damping could also induce the melting of crystals and modifies the Mathieu stability diagram [11].

Therefore, it is not obvious whether crystals can be formed at a high ac and with damping because (i) a high ac creates a strong focusing force, which pushes the ions closer and hence, the chaos-inducing Coulomb interaction [12] will be more dominant, and (ii) damping may also melt crystals [11].

As a result, while the two-ion case is the simplest crystal, it remains controversial as to what combinations of ac and dc allows the formation of two-ion crystals, under a range of damping values.

1.3 The Debate: Critical Transition at high AC

In July 1988, two papers [13, 14] on phase transitions of ions in a Paul Trap were published. Blümel *et al.* (hereafter the Munich group) reported the phase transitions between a chaotic cloud state of the ions and an ordered crystalline state, depending on the degree of laser cooling, while Hoffnagle, Brewer *et al.* (hereafter the IBM group) reported the order $\rightarrow$ chaos transition, or melting, of a two-ion crystal. Although both groups experimentally observed the transition from the crystal to the cloud state, they disagreed on the nature of such transitions. On one hand, for zero dc voltage, the Munich group found that there was no melting of ion crystals in molecular dynamics simulations within the stable trapping region (Mathieu stable), and that the ac voltage at which melting occurred in the experiments varied because of the effect of laser cooling. On the other hand, the IBM group claimed that in both experiments and simulations, a two-ion crystal melted at a critical high ac voltage, given constant damping. To summarize, the IBM group found an order $\rightarrow$ chaos transition at a critical ac value, while the Munich group found that the melting point varies as a function of cooling strength.

Subsequently, the Munich group responded with a detailed theoretical and experimental study [9], in which they showed that crystals could exist beyond the ac voltage claimed to exist by the IBM group. Moreover, results of the Munich group reflected that the Mathieu stability diagram gave an accurate prediction of the ac value that induces melting. They then suggested that the order $\rightarrow$ chaos

transition could be a result of perturbations from background gas collisions. The claim was corroborated by the fact that the Munich group then had a factor of six times lower background-gas pressure than the IBM group did. Thereafter, the IBM group came back with the observation of the transition under a pressure that was three times lower than the Munich group's [15]. They claimed, based on this observation, that the Munich group's conclusion that the melting transition would not occur at the critical ac voltage was clearly erroneous.

Over the next few years since then, the IBM group published various summary and review papers in the literature [12, 16–20], in which they assumed the transition to be true without further investigation. In [16–18], they showed that within a range of damping values, the transient lifetime, T, of two trapped ions before they crystallize obeyed a power law in the distance between the ac voltage being used and the claimed existence of a critical ac voltage. According to this theory, beyond the critical ac voltage, two trapped ions will take literally forever to crystallize, and hence, no two-ion crystal will form. However, this obviously conflicted with the Munich group's observation.

It was not until 1997 that the controversy was further addressed. This time, it was by a different group, Shen *et al.* (hereafter the Beijing group) [21]. From their numerical simulations, they found that the power-law behavior was true. However, their critical ac value was beyond the one claimed by the IBM group and could be predicted by the Mathieu stability diagram. By 2005, according to the literature, the controversy still remained [22]. Even to date, the controversy still stands, as there has been no other publication available in the literature addressing the controversy.

1.4 Outline

The objective of this thesis is to decisively resolve this controversy. In particular, we show both analytically and numerically that the crystals *exist* and they are *stable*, beyond the conjectured critical ac voltage. Thus, we prove that the IBM group's conjecture is false: the order $\rightarrow$ chaos transition in the Paul trap at the claimed critical ac voltage simply does not exist.

The outline of the thesis is as follows. Chapter 2 reviews the trapping principles of a hyperbolic Paul Trap. In Secs. 2.1 and 2.2, the theory of single-particle confinement in a Paul Trap is reviewed. In Sec. 2.4, we review the theory of multiple-particle confinement and introduce the two classes of stability: trap stability and crystal stability. In Sec. 2.5, we touch on the effect of damping. Chapter 3 presents the solution to the controversy. We resolve the controversy by showing that the crystal remains stable under the same parameters at which the IBM group claimed to have discovered the critical transition. In Secs. 3.1 and 3.2, we first establish that the crystal's center of mass is stable. Then, we prove numerically (see Secs. 3.1.1 and 3.2.1) and analytically (see Secs. 3.1.2 and 3.2.2) that the relative motion of the two trapped ions is stable. Chapter 4 discusses the possible sources of confusion that may have led the IBM group to its erroneous claims and started the controversy. In chapter 5, we present the implications of our results.

Chapter 2

Hyperbolic Paul Trap Theory

The aim of this chapter is to establish the theoretical foundation for stability in a Paul Trap, which is key to solving the controversy (see Secs. 1.2 and 1.3). In Sec. 2.1, we introduce the principles of single-particle confinement in a Paul Trap. In particular, the single-particle equations of motion will be derived in Sec. 2.2. Then in Sec. 2.3, based on the equations of motion, we will find which choices of the trap parameters, for instance, ac and dc voltages, lead to stable trapping. In Sec. 2.4, we first derive the multiple-particle equations of motion. Then, we focus on the center-of-mass (see Sec. 2.4.1) and relative motion (see Sec. 2.4.2) stabilities of multiple ions. Last but not least, the effect of damping in a Paul Trap will be presented in Sec 2.5.

2.1 Theory of single-particle confinement

The following discussion will be based on the dynamics of a single trapped ion. The theory can then be extended to multiple particles easily. The goal here is to

confine an ion in a three-dimensional space. In order to achieve that, a potential minimum needs to be created, which means there must exist a three-dimensional restoring force pointing to the minimum. By design, the forces will be directed to the center of the trap, where we want the ion to be trapped. Generally speaking, this force can assume many forms. However, the forces are required to be harmonic in order to obtain a simple analytical description of the motion of trapped ions. Therefore, in Cartesian coordinates, we have

$$F_u = -c_u u; \quad u = x, y, z, \tag{2.1}$$

where F_u is the focusing force in u-direction and $c_u > 0$ is a constant. The equation assumes that the center of the trap is at the origin, where the net force on the ion, averaged over many drive cycles, is zero.

In general, the relation between a force and its corresponding potential energy is given by

$$\vec{F} = -\vec{\nabla} U, \tag{2.2}$$

where $U = Q\Phi$ is the potential energy with Q being the charge of the ion and Φ being the electric potential that creates the force field. This, then, gives us the following relation for Φ in the Cartesian coordinates:

$$\Phi \sim (ax^2 + by^2 + cz^2), \tag{2.3}$$

where a, b, and c are some constants. Moreover, Φ has to satisfy Laplace's equation,

$$\nabla^2\Phi = 0, \tag{2.4}$$

which means the coefficients must satisfy $a + b + c = 0$. The case of rotational symmetry around the z-axis requires $a = b$ and, hence, $c = -(a + b)$. By setting $a = 1$, (2.3) becomes

$$\Phi \sim (x^2 + y^2 - 2z^2). \tag{2.5}$$

Notice that the potential will have a minimum in the x- and y-coordinate, but a maximum in the z-coordinate, thus, creating a saddle point at the origin. If the ion is placed at the origin and the electric field is switched on, the ion will oscillate in the x-y plane but its displacement in the z-direction will increase exponentially and quickly end up hitting an electrode. Thus, the attempt to generate an electrostatic confining field has failed. This is not surprising since, after all, Earnshaw's theorem [23] states that it is impossible to create a minimum of an electrostatic potential in free space.

A solution to this problem is a periodic electrodynamic potential. As the sign of the electric force switches periodically, the radial and axial forces alternate between focusing and defocusing, and the two forces are never simultaneously focusing or defocusing. In general, the applied voltage to the Paul Trap electrodes is of the form

$$\Phi_0 = U_0 + V_0 \cos(\Omega t), \tag{2.6}$$

where U_0, V_0 and Ω represent the dc voltage, ac (or rf) voltage and driving frequency respectively. Then, the electric potential at the center of the trap may be

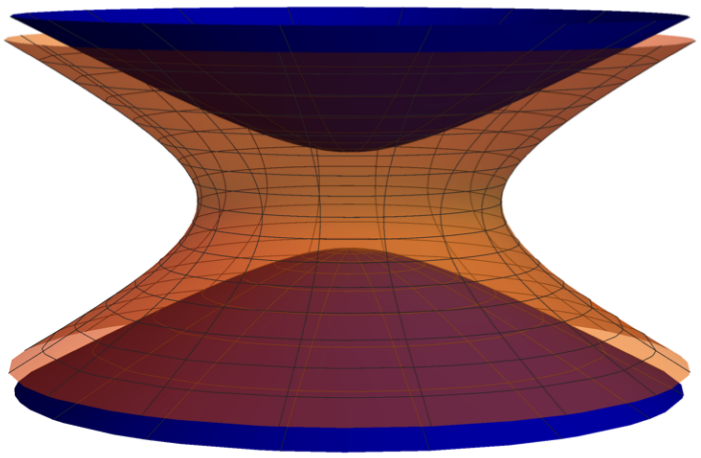

Figure 2.1: The setup of the electrodes of a Paul Trap.

written down as

$$\begin{aligned}\Phi &= \frac{\Phi_0}{r_0^2 + 2z_0^2}(x^2 + y^2 - 2x^2) \\ &= \frac{U_0 + V_0\cos(\Omega t)}{r_0^2 + 2z_0^2}(x^2 + y^2 - 2x^2),\end{aligned} \tag{2.7}$$

where $2z_0^2 = r_0^2$; Here, z_0 and r_0 are the dimensions of the trap: z_0 is the shortest distance between the center of the trap and either of the end-cap electrodes; r_0 is the shortest distance between the center of the trap and the ring electrode. As shown in Fig. 2.1 [24], this potential is produced by applying the voltage across a hyperbolic ring electrode (orange) and a pair of hyperbolic cap electrodes (blue).

The shape of the equipotential surface, for the case of $U_0 = 0$ and $y = 0$ with T as the oscillation period, is shown in Figs. 2.2(a) and 2.2(b). At $t = 0$ the potential at origin is at minimum in the x-coordinate and maximum in the z-coordinate, and the coordinates of the potential minimum and maximum switch

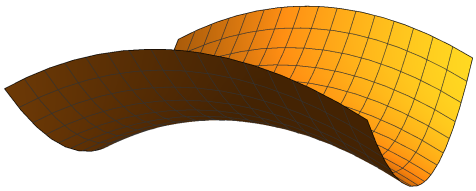

(a) $t = 0$

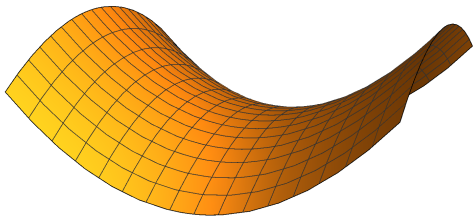

(b) $t = T/2$

Figure 2.2: The saddle-shaped equipotential surface in a Paul Trap.

at $t = T/2$.

To help understand the dynamic stabilization in a Paul Trap, we consider Wolfgang Paul's mechanical analogue device [1], which consists of a small ball placed about the saddle point of the surface shaped as in Figs. 2.2(a) and (b). If the surface stays still, the ball will roll off in the convex direction, implying instability. However, if the surface rotates with about a vector normal to the saddle point, it becomes possible that the ball may remain near the saddle point of the surface for a long time, implying stability. This is so, because the ball, heading towards the originally unstable, convex direction, may be countered by the now concave stable direction, resulting from the rotation of the surface. Moreover, depending on the steepness of the surface, the range of frequencies that leads to stability changes. The steeper the surface, the faster the ball rolls off, which means the range of frequencies needs to be higher in order to catch the ball before it rolls

off.

Referring back to the trap, since the trapping electric field is inhomogeneous, the average force on the charged particle over many cycles may not be zero. In particular, it becomes possible that the average force points towards the center of the trap. Whether or not the averaged force on the charged particle is convergent to the center of the trap depends on the magnitude and frequency of the oscillating field. Therefore, despite the constant alternation between focusing and defocusing of the ion in each direction caused by the electrodynamic field, it is possible, with an appropriate combination of field magnitude and frequency, to generate a time-averaged restoring force in all three dimensions towards the center of the trap, resulting in confinement.

2.2 Single-Particle Equation of Motion

One can obtain the conditions for stable confinement of a charged particle with charge Q and mass m in a Paul Trap by solving the single-particle equation of motion:

$$m\frac{d^2}{dt^2}\begin{bmatrix} x \\ y \\ z \end{bmatrix} + 2Q\frac{U_0 - V_0\cos(\Omega t)}{r_0^2 + 2z_0^2}\begin{bmatrix} x \\ y \\ -2z \end{bmatrix} = 0. \tag{2.8}$$

In dimensionless trap parameters a and q defined by,

$$a = \frac{8QU_0}{m\Omega^2(r_0^2 + 2z_0^2)}, \tag{2.9}$$

and

$$q = \frac{4QV_0}{m\Omega^2(r_0^2 + 2z_0^2)}, \tag{2.10}$$

and dimensionless time unit τ, defined by,

$$\tau = \frac{\Omega t}{2}, \tag{2.11}$$

(2.8) may be transformed into the dimensionless equation of motion of a single particle in a Paul Trap:

$$\frac{d^2}{d\tau^2}\begin{bmatrix} x \\ y \\ z \end{bmatrix} + [a - 2q\cos(2\tau)]\begin{bmatrix} x \\ y \\ -2z \end{bmatrix} = 0. \tag{2.12}$$

This transform, known as nondimensionalization, is a commonly used theoretical technique when analyzing physical systems, because it simplifies the analysis and parameterization of a system by removing scales and shrinking the parameter space. In the case of a Paul Trap, the trap parameter space is reduced from seven dimensions, i.e., Q, U_0, V_0, r_0, z_0, m and Ω, to two dimensions, i.e., q and a. Yet there is no loss of information due to nondimensionalization as the dependence on the seven parameters is encoded into that on the two parameters. More specifically, changing a (or q) embodies an individual change in any of the seven parameters that a (or q) is dependent on, or a collective change in any combination of them. For example, doubling a implies doubling Q or doubling the ratio between U_0 and m.

In addition, in its dimensionless form, one can easily recognize that (2.12) is a system of three Mathieu's Equation [25]. The radial equations are already

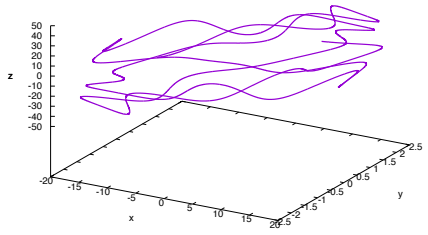

Figure 2.3: The motion of a trapped particle over twenty drive cycles.

of the canonical form. By letting $a \to -2a$ and $q \to -2q$, the axial equation is transformed into the canonical form. This is an important realization since the well-known analytical solution of a Mathieu's Equation gives us an exact description of the motion of a trapped particle.

Before going through the steps of solving the set of Mathieu's Equations exactly, we may first visualize the motion of the trapped particle through numerical simulations. A sample motion of a charged particle in a Paul trap may be obtained by tracing the position of the particle over time, as in Fig. 2.3.

While the motion of the particle may seem wildly random, it is actually determined entirely by the initial condition of the system because the particle's equations of motion imply that a Paul Trap is a deterministic system. In a deterministic system, there is no (stochastic) randomness involved in the evolution of the system, which means that, in principle (chaos may change this in practice), an initial state will always produce the same future states. In our single-particle Paul Trap system, the initial state, represented by the initial phase-space vector

$$\vec{X}_0 = (x_0, y_0, z_0, \dot{x_0}, \dot{y_0}, \dot{z_0}), \tag{2.13}$$

and the phase-space vector's time-derivative,

$$\frac{d}{dt}\vec{X} = \vec{F}(\vec{X}, t), \tag{2.14}$$

where $\vec{F}$ denotes a function of $\vec{X}$ and t, uniquely determine the particle's future states.

Moreover, the fact that the equations of motion are linear, indicates that the single-particle motion will never be chaotic. A full analytical expression for $\vec{X}$ at any time t can be obtained via solving the system of Mathieu's equation [25].

2.3 Stability Diagram

Given an analytical expression for the trajectory of a particle, $\vec{X}(t)$, we may now determine whether the particle remains confined in a Paul Trap. To do so, we first classify the trajectories of a charged particle in a Paul trap as follows:

Let $\delta(t)$ be the particle's distance from the center of the trap and Γ be some arbitrary positive real number.

(1) *Bounded Trajectory*: $|\delta(t)| < \Gamma$, for all t. In this case, the particle forever stays within a distance Γ from the center of the trap.

(2) *Unbounded Trajectory*: For any $\Gamma > 0$, $|\delta(t)| > \Gamma$, for all $t > t^* > 0$. This means that given enough time the particle will move infinitely far away from the center of the trap.

Obviously, a stably trapped particle will have a bounded trajectory and a not stably trapped particle will have an unbounded trajectory.

We mentioned in Sec. 2.1 that an appropriate combination of field magnitude and frequency, embodied by q and a (see Sec. 2.2), will lead to particle confinement. In the remaining part of this section, we determine which choices of (q, a) lead to stability.

In order to achieve three-dimensional trapping, both radial and axial stability are necessary. Since in the single-particle case x- and y-coordinates are decoupled, considering the radial stability is equivalent to considering stability in the x-direction. Therefore, we focus on

$$\ddot{x} + [a - 2q\cos(2\tau)]x = 0, \tag{2.15}$$

Since (2.15) is a linear, second-order differential equation for r, with time-periodic coefficients, Floquet theory [25, 26] tells us that the solutions of (2.15) are of the form

$$f(\tau) = e^{i\mu(q,a)\tau}F(\tau), \tag{2.16}$$

where $\mu(q, a)$ is determined by the trap parameters (q, a) and

$$F(\tau) = F(\tau + T) \tag{2.17}$$

is a periodic function of the same period $T = \pi$ as the drive. We then deduce that if $\mu(q, a)$ is real, the solution $f(\tau)$ is stable; if $\mu(q, a)$ is complex, with a negative imaginary part, the solution $f(\tau)$ is unstable because $|f(\tau)|$ increases exponentially in time.

Using $f(\tau)$, we construct two real solutions to (2.15), the Mathieu cosine $C(\tau)$ and sine $S(\tau)$ solutions, i.e.,

$$C(\tau) = \frac{1}{2}(f(\tau) + f(-\tau)), \tag{2.18}$$

and

$$S(\tau) = \frac{1}{2i}(f(\tau) - f(-\tau)). \tag{2.19}$$

Next, we exploit the result from Appendix A that when μ is an integer, the general solution consists of one periodic solution (π- or 2π-periodic) and a second linearly-independent solution is unstable (see (A.7)). In this case, we let $\mu = 2k+n$, where k and n are integers. Then, $f(\tau), C(\tau)$, and $S(\tau)$ becomes the following:

$$f(\tau) = \sum_{k=-\infty}^{\infty} c_{2k+n} e^{i(2k+n)\tau}, \tag{2.20}$$

$$C(\tau) = \sum_{k=-\infty}^{\infty} c_{2k+n} \cos[(2k+n)\tau], \tag{2.21}$$

and

$$S(\tau) = \sum_{k=-\infty}^{\infty} c_{2k+n} \sin[(2k+n)\tau]. \tag{2.22}$$

The reason why we rewrite μ as $2k + n$ is the following: For a given value of q, the radial equation of motion (2.15) admits a discrete set of $a's$ that yields solutions of the form (2.21), and another discrete set of $a's$, denoted as $b's$, that yields solutions of the form (2.22). Each element of the two discrete sets, a_n and

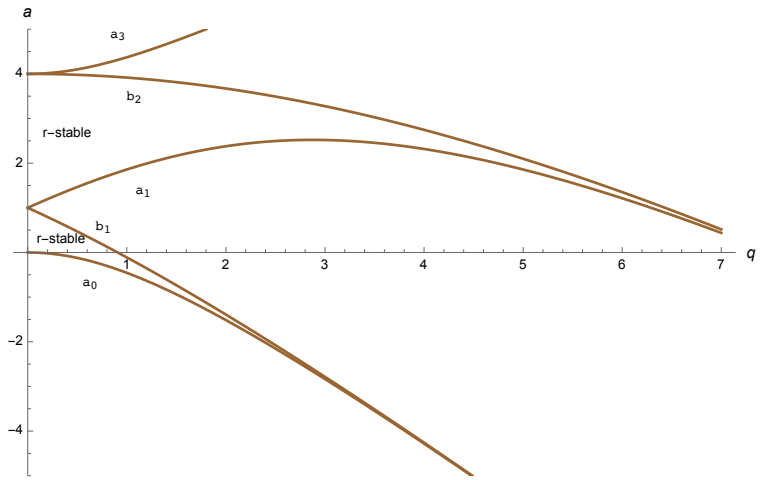

Figure 2.4: The radial stability regions

b_n, varies continuously as a function of q and produces the *characteristic curves*, $a_0, b_1, a_1, b_2...$, in the (q, a) parameter space. The analytic expressions of these curves can be obtained by plugging (2.21) and (2.22) into (2.15) [25].

In fact, these characteristic curves are the boundaries between stable and unstable regions of the parameter space because the (q, a)'s on them lead to solutions that could be periodic or unstable. Apparently, the (q, a) points between a_n and b_{n+1} correspond to the stable solutions with real and non-integer μ's. Therefore, the regions labeled *r-stable* in Fig. 2.4 yield stable solutions of the radial equations of motion (2.15). On the other hand, the unlabeled regions outside the curves in Fig. 2.4 correspond to the unstable solutions with μ that are complex with negative imaginary parts. Finally, the (q, a) values, which yield periodic solutions (2.21) and (2.22), produce the characteristic curves that are the transition between the stable and unstable solutions.

We can easily obtain the axial stability regions illustrated in Fig. 2.5 by applying the transformation $(q, a) \rightarrow (-2q, -2a)$ to the radial characteristic curves. Essen-

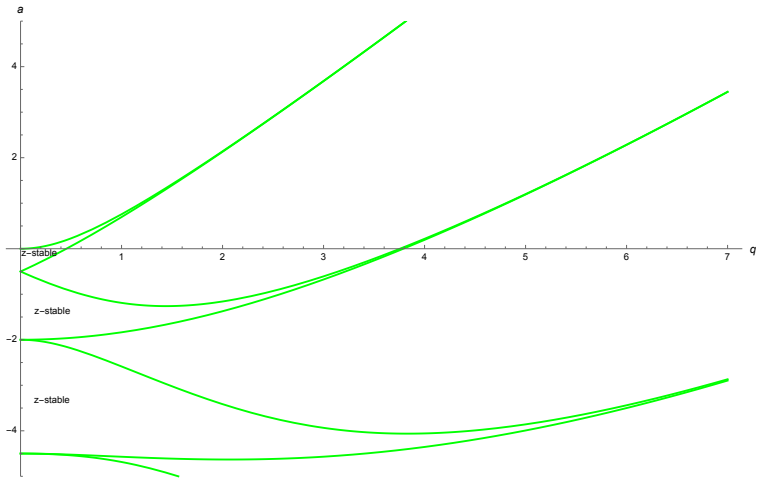

Figure 2.5: The axial stability regions

tially, the axial stability curves are flipped about the q-axis and compressed by a factor $\frac{1}{2}$.

The (q, a) points that lead to three-dimensional trapping lie in the regions that are both radially and axially stable. While there are many of such regions in the parameter space, ion-trap physicists are most interested in the region nearest to the origin, known as the Mathieu stability diagram (see Fig. 2.6), since lower (q, a) settings are more experimentally realistic and achievable. Therefore, from here on and in the following, throughout this thesis, we consider only those (q, a) values that lie in the Mathieu stability diagram as well.

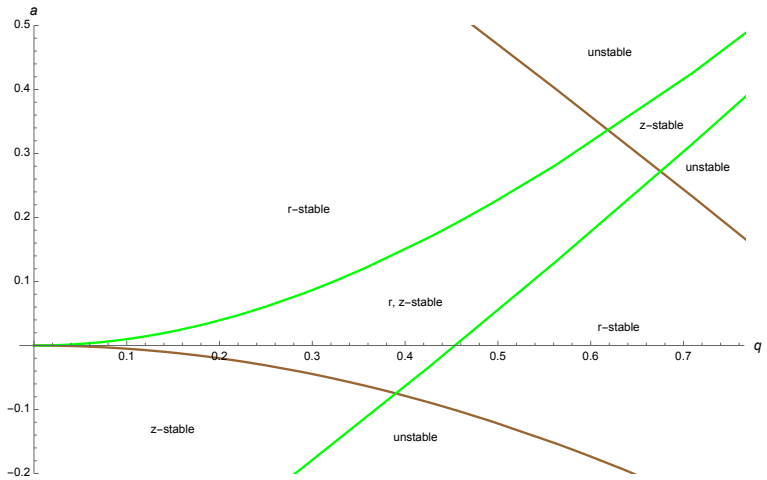

Figure 2.6: The Mathieu stability diagram

2.4 Multiple-Particle Equations of Motion

If there are more than one particle in a Paul Trap, the Coulomb interactions between the particles has to be taken into consideration in the equations of motion. The Coulomb force acting on particle i caused by particle j, can be written as

$$\vec{F}_{coul}^{(i,j)} = \frac{1}{R_{ij}^3} \begin{bmatrix} x_i - x_j \\ y_i - y_j \\ z_i - z_j \end{bmatrix}, \tag{2.23}$$

where $R_{ij} = [(x_i - x_j)^2 + (y_i - y_j)^2 + (z_i - z_j)^2]^{\frac{1}{2}}$ is the distance between particles i and j.

The differential equations describing the motion of the trapped particles are thus coupled through the non-linear Coulomb term, which may lead to chaos. Using (2.23) and the single-particle equation of motion (2.12), we obtain the equation of motion of one of the trapped particles

$$\frac{d^2}{d\tau^2}\begin{bmatrix} x_i \\ y_i \\ z_i \end{bmatrix} + [a - 2q\cos(2\tau)]\begin{bmatrix} x_i \\ y_i \\ -2z_i \end{bmatrix} = \sum_{i\neq j} \vec{F}_{coul}^{(i,j)}. \tag{2.24}$$

2.4.1 Trap Stability

We note that the Mathieu stability diagram derived for the single-particle case (see Fig. 2.6) is still valid for determining the stability of the center of mass of the particles, denoted as the *trap stability*, because the Coulomb terms drop out in the center-of-mass coordinates. Considering for instance a two-particle case, in order to switch to the center-of-mass coordinates, we add the equations of motion for particles i and j. It is straightforward to show that, in this case, the Coulomb forces $\vec{F}_{coul}^{(i,j)}$ and $\vec{F}_{coul}^{(j,i)}$ cancel each other out, expectedly so, according to Newton's third law. If we now consider N trapped particles pair by pair and apply the aforementioned reasoning, we arrive at the center-of-mass equation, which, after rescaling, is equivalent to the single-particle equation. In other words, the multiple-particle stable trapping condition is the same as that of a single particle. A qualitative and more intuitive explanation for that is that while the magnitude of the repulsive Coulomb forces falls off according to the inverse-square law, while the trap force on each particle increases linearly with the distance from the trap center, thereby completely overpowering the Coulomb repulsion.

2.4.2 Crystal Stability

Even though chaos may emerge from the non-linear Coulomb coupling, it has been shown that the trapped particles may form crystals, an ordered state where

the particles' phase space vector appears stroboscopically constant after each trap cycle. Crystals in a Paul Trap are interesting because they allow experimentalists to investigate complicated few-body dynamics with high precision.

To form a stable crystal, the particles need to have stable center-of-mass motion and stable relative motion. However, it is almost impossible to determine the relative motion stability, or *crystal stability*, analytically because the dynamics of the particles are described by a high-dimensional phase-space vector. Moreover, the nonlinear differential equations cannot be conveniently separated in the relative coordinates. Therefore, we turn to numerical simulation. For our simulations, we use the fifth-order Runge-Kutta method. While the Runge-Kutta method and the finite computer precision may lead to errors in simulations, these sources of error are insignificant. In other words, our simulations provide data that realistically capture the dynamics of trapped particles. Therefore, the phase space of the particles can be accessed to determine the crystal stability in the trap.

It is important to notice that trap stability and crystal stability are separate criteria, and that there is no causation between them. In fact, it was numerically shown that, within the Mathieu stability diagram, there are regions in which crystals cannot be formed [10, 27]. Moreover, in Ch. 3, we will show analytically and numerically that particles can lose trap stability, but maintain crystal stability.

2.5 Damping

Until now, we have only considered the undamped dynamics of particles in a Paul Trap. However, in experiments, Paul traps are always used in tandem with various

cooling techniques. Therefore, we must add damping into our theory to make it more realistic. We assume that damping has a linear effect on the velocity of the trapped particles, which is an excellent model for common cooling methods such as laser or buffer gas cooling [9, 16]. Thus, the damped equation of motion for a trapped particle can be written as

$$\frac{d^2}{d\tau^2}\begin{bmatrix} x_i \\ y_i \\ z_i \end{bmatrix} + \gamma\frac{d}{dt}\begin{bmatrix} x_i \\ y_i \\ z_i \end{bmatrix} + [a - 2q\cos(2\tau)]\begin{bmatrix} x_i \\ y_i \\ -2z_i \end{bmatrix} = \sum_{i\neq j}\vec{F}^{(i,j)}_{coul}, \tag{2.25}$$

where γ is the damping coefficient.

Intuitively, damping increases the stability of the trapped particles. However, this is not always the case as it was shown that damping modifies the Mathieu stability diagram [11]. In particular, damping squeezes the stability curves in the a-direction, and stretches them in the q-direction. Moreover, as damping reaches a critical level at a fixed (q, a), it can induce the melting of crystals [11].

Chapter 3

Solution to the Controversy

Since the detailed chronological recount of the controversy can be found in Ch. 1, we shall give a quick summary of where the controversy now stands based on the technical terms developed in Ch. 2. The controversy centers on the order $\rightarrow$ chaos transition, or melting, of a two-ion crystal at $a = 0$. On one hand, the Munich group observed experimentally that the transition happens at various q values [13]. On the other hand, the IBM group found in their experiments that the transition occurs at a critical q value, denoted as q_c [14]. The Munich group justified via simulations and experiments [9] that crystals could exist beyond the claimed q_c until the Mathieu Instability, denoted as q_{MI}. They suggested that the transition was induced by *noise*. However, the IBM group claimed that the transition was experimentally and numerically *reproducible*, and was *deterministic* [18]. In [16–18], they proposed that the transient lifetime, T, of two trapped ions before their crystallization obeyed a power law in the distance between the trap parameter q and the critical parameter q_c, i.e., $T \propto |q_c - q|^{-k}$. A precise value of q_c was quoted in [18], e.g., $q_c = 0.87$ ($q_c = 0.435$ in our nomenclature) when

the damping parameter γ was within 0 and 1×10^{-3}, and $a = 0$. While the Beijing group reproduced the power law numerically, they found that $q_c \approx q_{MI}$ [21], which supported the Munich group's claim that the crystals could exist until $q_{MI} = 0.454023$. Since then, there has been no other publication that attempts to resolve the controversy.

In this chapter, we solve the controversy in two cases, the undamped case (see Sec. 3.1 and the damped case (see Sec. 3.2). For each case, we first establish that the two-ion crystal's center of mass is stable until q_{MI}. Then, we semi-analytically (see Secs. 3.1.1 and 3.2.1) and analytically (see Secs. 3.1.2 and 3.2.2) show that its relative motion is stable, beyond the conjectured $q_c = 0.435$. Thereby, we conclude that crystals exist until q_{MI} and hence, the order $\rightarrow$ chaos transition is proven to be noise-induced, and not deterministic.

3.1 Undamped case

In order to prove the stability of a two-ion crystal, we need to show that the crystal's center of mass and relative motion are stable. We first consider the case of zero damping. Based on the discussion in Ch. 2.4.1, we can conclude that the crystal's center-of-mass motion is stable until q_{MI} is reached. We now prove that the equation of motion in the relative coordinates for a two-ion crystal on the $x - z$ plane, for $a = 0$,

$$\frac{d^2}{dt^2}\begin{bmatrix} x \\ z \end{bmatrix} + [-2q\cos(2t)]\begin{bmatrix} x \\ -2z \end{bmatrix} = (x^2 + z^2)^{-\frac{3}{2}}\begin{bmatrix} x \\ z \end{bmatrix}. \tag{3.1}$$

has a fixed point, which is stable until (and beyond) q_{MI} is reached. The most

straightforward method is to show that (3.1) is *Lyapunov stable* using the *Lyapunov stability criterion* [28]. However, the construction of a Lyapunov function for complicated systems, such as (3.1), requires immense experience, and hence, attempts to do so are almost always futile. Instead, we do this by linearizing and separating (3.1), and using Floquet theory [25, 26]. Note that we use t instead of τ in (3.1) only for the sake of convenience. We write (3.1) with a cosine drive term since (i) this is the canonical form of Mathieu's equation [25], which forms the left-hand side of (3.1), and (ii) in this case the solutions of (3.1) can be classified into even and odd with respect to $t \to -t$. If the drive term is $\sin(2t)$, or in general, $\cos(2t + \alpha)$, where α is a real constant, a simple shift of the origin of time will carry the new drive term into the $\cos(2t)$ term used in (3.1).

We begin our analysis of (3.1) by defining $x_f(t)$ as the period-1 solution of the radial part of (3.1), i.e., $x(t + T) = x(t)$, where $T = \pi$ is the period of the drive term in (3.1). By necessity, $x_f(t)$ is an even solution of (3.1), since an odd solution would imply that $x_f(t)$ is zero at $t = 0$. However, this is impossible since $x(t)$ in (3.1) represents the distance between the two ions of the crystal, and $x_f(t = 0) = 0$ would mean a vanishing distance between the two ions with a corresponding infinite Coulomb interaction energy.

Now, we introduce a perturbed solution of the x-component of (3.1), $g(t)$, which initially is close to $x_f(t)$, i.e., $|g(t = 0) - x_f(t = 0)| < \epsilon$, where ϵ is small and positive, and prove that, in linear order, $|g(t) - x_f(t)| < \delta$ for all t and all $q < q_{max}$, where $q_{max} > q_{MI}$. This will prove that the cycle $x_f(t)$ is stable not just up to the Mathieu instability, as claimed in [9], but even beyond.

We define

$$g(t) = x_f(t) + w(t). \tag{3.2}$$

Since $g(t)$, by definition, satisfies (3.1), we obtain

$$\frac{d^2}{dt^2}\begin{bmatrix} x_f + w \\ z \end{bmatrix} + [-2q\cos(2t)]\begin{bmatrix} x_f + w \\ -2z \end{bmatrix} = ((x_f + w)^2 + z^2)^{-\frac{3}{2}}\begin{bmatrix} x_f + w \\ z \end{bmatrix}. \tag{3.3}$$

Note that $a = 0$ produces planar crystals in the xy plane. In other words, the axial motion is already small, i.e., on the order of w, and acts as a perturbation. Therefore, there is no need to introduce a perturbation in the axial part of (3.3).

We then linearize and separate the radial and axial parts of (3.3) (see Appendix C), and obtain:

$$\ddot{w} + [\frac{2}{x_f^3} - 2q\cos(2t)]w = 0 \tag{3.4}$$

for the radial part, and

$$\ddot{z} + [\frac{-1}{x_f^3} + 4q\cos(2t)]z = 0 \tag{3.5}$$

for the axial part.

3.1.1 Semi-analytical Approach

Both (3.4) and (3.5) are linear, second-order differential equations for $w(t)$ and $z(t)$, respectively, with time-periodic coefficients for which Floquet theory [25, 26]

holds. This theory asserts that the solutions of (3.4) are of the form

$$w(t) = e^{i\mu_w(q)t}W(t), \tag{3.6}$$

where $\mu_w(q)$ is a q-dependent constant and

$$W(t) = W(t+T) \tag{3.7}$$

is a periodic function of period T. In a similar fashion, the solutions of (3.5) are of the form

$$z(t) = e^{i\mu_z(q)t}Z(t), \tag{3.8}$$

where $\mu_z(q)$ is a q-dependent constant and

$$Z(t) = Z(t+T). \tag{3.9}$$

The exponential term in (3.6) (or (3.8)) is denoted as the *characteristic multiplier* of (3.4) (or (3.5)). We then conclude that if both $\mu_w(q)$ and $\mu_z(q)$ are real, the cycle $x_f(t)$, and hence, the two-ion planar crystal, are stable. If any of $\mu_w(q)$ and $\mu_z(q)$ is complex, with a negative imaginary part, the cycle $x_f(t)$ is unstable because in this case $|w(t)|$ increases exponentially in time.

We then numerically determine the stability of the cycle $x_f(t)$. First, we define a 2×2 mapping matrix $\mathbf{A}(q)$ such that

$$\mathbf{A}(q)\begin{pmatrix} w(t) \\ \dot{w}(t) \end{pmatrix} = \begin{pmatrix} w(t+T) \\ \dot{w}(t+T) \end{pmatrix}, \tag{3.10}$$

where $T = \pi$ is the period of the drive term, and $\mathbf{A}(q)$ is a function of q. All the matrix entries of $\mathbf{A}(q)$, for a fixed q, can be obtained numerically by solving (3.4) for one period using the initial conditions, $\begin{pmatrix} 1 \\ 0 \end{pmatrix}$ and $\begin{pmatrix} 0 \\ 1 \end{pmatrix}$. Then, we vary the value of q to obtain $\mathbf{A}(q)$ at various q's. Hereafter, we write $\mathbf{A}(q)$ as $\mathbf{A}$.

Now, we claim that for a system, to which Floquet theory is applicable, its mapping matrix M has eigenvalues that are its characteristic multipliers with $t = T$.

Proof:

First, let the system be described by a periodic linear differential equation:

$\dot{\vec{y}}(t) = \mathbf{P}(t)\vec{y}(t)$,

where $\mathbf{P}(t)$ is a periodic function with period T.

By Floquet theory [26], the solutions are of the form

$\vec{y}(t) = e^{i\mu t}\vec{Y}(t)$, where $\vec{Y}(t) = \vec{Y}(t+T)$.

Then, we apply $\mathbf{M}$ to a solution $\vec{y}_i(t)$

$\mathbf{M}\vec{y}_i(t) = \vec{y}_i(t+T) = e^{i\mu_i(t+T)}\vec{Y}_i(t+T) = e^{i\mu_i(t+T)}\vec{Y}_i(t) = e^{i\mu_i T}\vec{y}_i(t)$

Therefore, $\mathbf{M}$ has eigenvalues $e^{i\mu_i T}$ as claimed.

(3.11)

(3.11) implies that the eigenvalues of the matrix $\mathbf{A}$ tell us the stability of (3.6), and hence, the stability of the two-ion crystal. Therefore, we now obtain the eigenvalues, $\lambda_\pm$, of $\mathbf{A}$ by diagonalization. Then, we get

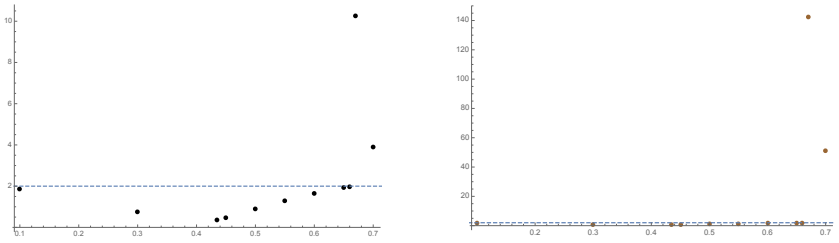

(a) $Tr(\mathbf{A}(q))$ is plotted as a function of q. The dashed lines represents $Tr(\mathbf{A}(q)) = 2$.

(b) $Tr(\mathbf{B}(q))$ is plotted as a function of q. The dashed lines represents $Tr(\mathbf{B}(q)) = 2$.

Figure 3.1: $Tr(\mathbf{A}(q))$ and $Tr(\mathbf{B}(q))$ are plotted as a function of q.

$$\lambda_{\pm} = \frac{Tr(\mathbf{A}) \pm \sqrt{Tr(\mathbf{A})^2 - 4Det(\mathbf{A})}}{2} \tag{3.12}$$

where $Tr(\mathbf{A})$ is the trace of $\mathbf{A}$, and $Det(\mathbf{A})$ is the determinant of $\mathbf{A}$,

However, by Liouville's Theorem, since our system described by (3.4) is Hamiltonian, $Det(\mathbf{A}) = 1$ [29]. So,

$$\lambda_{\pm} = \frac{Tr(\mathbf{A}) \pm \sqrt{Tr(\mathbf{A})^2 - 4}}{2}. \tag{3.13}$$

So, we conclude if $|Tr(\mathbf{A})| < 2$, then $\lambda_{\pm}$ are complex, with λ_+ and λ_- being complex conjugates, and furthermore, the norm of $\lambda_{\pm}$ is 1, meaning that the Floquet exponents in (3.6) are real. In other words, given that $|Tr(\mathbf{A})| < 2$, the crystal is stable. For the axial motion, we can obtain a mapping matrix $\mathbf{B}(q)$ and apply the same stability analysis to it. $Tr(\mathbf{A})$ and $Tr(\mathbf{B})$ are plotted as a function of q in Fig. 3.1.

$Tr(\mathbf{A}) > 2$ at $q = 0.67 > q_{MI} = 0.454023$ and $Tr(\mathbf{B}) > 2$ at $q = 0.67 > q_{MI}$. Surprisingly, at q_{MI}, the crystal does not become unstable in the trap because of

instability in the relative motion, but rather, of instability of the center-of-mass motion, which turns unstable precisely at $q = q_{MI}$. Therefore, the two-ion planar crystal exists until q_{MI}.

3.1.2 Analytical Approach

The proof presented in Sec. 3.1.1 is rigorous, but it rests on the assumption that the numerical calculations were executed correctly. Therefore, in this section, we present analytical estimates that corroborate the results presented in Sec. 3.1.1. In order to make contact with established methods used in the ion-trapping community, we base our analytical estimates on the pseudopotential method, a standard analytical method used frequently in the literature to estimate size and configurations of ion crystals in the Paul trap [30–32]. Our analytics consist of three parts: First, we assume $x_f(t)$ to be (i) constant; then, since $x_f(t)$ is a π-periodic function of time, it is possible to expand $x_f(t)$ in a (ii) Taylor series and (iii) Fourier series.

Pseudopotential

The pseudopotential method is based on the insight that the solutions of (3.1) consist of a slow, guiding-center macro-motion $X(t)$, and a fast vibrating micro-motion $\xi(t)$. To support the insight, we simulated the motion of a trapped particle. The motion, with and without micro-motion, of the particle is obtained by plotting the position of the particle continuously, as in Fig. 3.2a, and at the end of each drive cycle, as in Fig. 3.2b. Indeed, we see from Fig. 3.2 that the particle's motion is a superposition of the micro- and macro-motion.

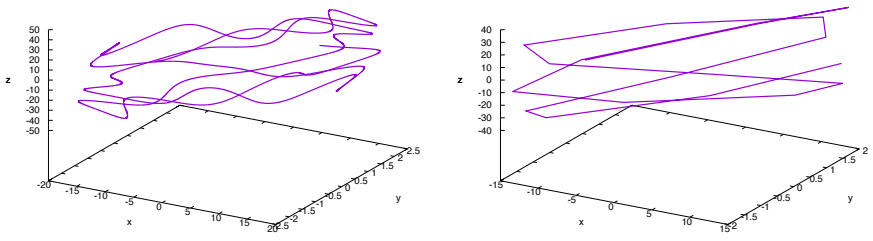

(a) Macro- and micro-motion over twenty trap cycles.

(b) Macro-motion over twenty trap cycles.

Figure 3.2: The motion, with and without micro-motion, of a charged particle in a Paul Trap.

We may now write

$$x(t) = X(t) + \xi(t). \tag{3.14}$$

Defining the cycle average of a function $f(t)$ according to

$$\langle f(t) \rangle = \frac{1}{\pi} \int_{-\frac{\pi}{2}}^{\frac{\pi}{2}} f(t + t')dt', \tag{3.15}$$

the pseudopotential method assumes

$$\langle X(t) \rangle \approx X(t), \quad \langle \xi(t) \rangle = 0; \tag{3.16}$$

$$|X(t)| \gg |\xi(t)|, \quad |\ddot{X}(t)| \ll |\ddot{\xi}(t)|. \tag{3.17}$$

Since we are investigating the case of a planar crystal in the $z = 0$ plane, we may obtain the analytical approximation of $x_f(t)$ by considering only the radial part of (3.1) with $a = 0$ and $z = 0$. Plugging in $a = 0$ and $z = 0$ into the x-component of (3.1), we obtain

$$\ddot{x}(t) - 2q\cos(2t)x(t) = \frac{x(t)}{|x(t)|^3}. \tag{3.18}$$

Pseudopotential analysis of (3.18) consists of two steps. The first step, neglecting the right-hand side of (3.18), focuses on the left-hand side of (3.18), i.e., the Mathieu's equation

$$\ddot{x}(t) - 2q\cos(2t)x(t) = 0, \tag{3.19}$$

and constructs an effective potential, $U_{eff}(X)$, in which $X(t)$ moves. The second step, considering force equilibrium between

$$F_{eff} = -\frac{dU_{eff}(X)}{dX} \tag{3.20}$$

and the Coulomb-repulsion force, $\frac{1}{r(t)^2}$ (the right-hand side of (3.18)), determines the location of the equilibrium distance of the ions of the crystal.

Inserting (3.14) into (3.19), and, by (3.17), neglecting $\ddot{X}(t)$ with respect to $\ddot{\xi}(t)$, and $\xi(t)$ with respect to $X(t)$, we arrive at an approximate equation for $\xi(t)$ according to

$$\ddot{\xi}(t) = 2q\cos(2t)X(t). \tag{3.21}$$

Assuming that, in accordance with (3.17), $X(t)$ is essentially constant over one cycle of the drive in (3.14), we may then integrate (3.21) to obtain

$$\xi(t) = -\frac{q}{2}\cos(2t)X(t). \tag{3.22}$$

Considering the cycle-averaged (3.19), we obtain

$$\langle \ddot{X}(t)\rangle + \langle \ddot{\xi}(t)\rangle - 2q[\langle \cos(2t)X(t)\rangle + \langle \cos(2t)\xi(t)\rangle] = 0. \tag{3.23}$$

As a result of (3.22), we have

$$\langle \ddot{\xi}(t)\rangle = 0, \quad \langle \cos(2t)\xi(t)\rangle = -\frac{q}{4}, \tag{3.24}$$

and due to the assumption of near-constancy of $X(t)$ over a cycle, we may write

$$\langle \cos(2t)X(t)\rangle \approx 0. \tag{3.25}$$

Inserting (3.24) and 3.25 into (3.23), we end up with the approximation

$$\ddot{X}(t) = -\frac{q^2}{2}X(t). \tag{3.26}$$

Hence, we may imagine that X moves in a fictitious potential,

$$U_{eff} = \frac{q^2}{4}X^2, \tag{3.27}$$

from which the force acting on X is derived using 3.20. According to this analysis, the location of the fixed point $\tilde{x_f}$, i.e., the mid-point of $x_f(t)$, is now obtained from the condition of force equilibrium between F_{eff} and $\frac{1}{r(t)^2}$ according to

$$\frac{q^2}{2}\tilde{x}_f = \frac{1}{\tilde{x}_f^2}, \quad \rightarrow \tilde{x}_f = (\frac{2}{q^2})^{\frac{1}{3}}. \tag{3.28}$$

Along with (3.14) and (3.29), we finally obtain an approximate result for $x_f(t)$:

$$x_f(t) \approx \tilde{x}_f + \xi(t) = (\frac{2}{q^2})^{\frac{1}{3}}[1 - (\frac{q}{2})\cos(2t)]. \tag{3.29}$$

Assume constant $x_f(t)$: As a first step, we assume $x_f(t) = \tilde{x}_f$. Then, we plug (3.28) into (3.4) and (3.5) to obtain

$$\ddot{w} + [q^2 - 2q\cos(2t)]w = 0 \tag{3.30}$$

and

$$\ddot{z} + [-\frac{q^2}{2} + 4q\cos(2t)]z = 0, \tag{3.31}$$

respectively. Then, we rewrite (3.30) as a Mathieu's equation in the form

$$\ddot{w} + [\tilde{a}_w - 2\tilde{q}_w\cos(2t)]w = 0, \tag{3.32}$$

where

$$\tilde{q}_w = q, \quad \tilde{a}_w = \tilde{q}_w^2, \tag{3.33}$$

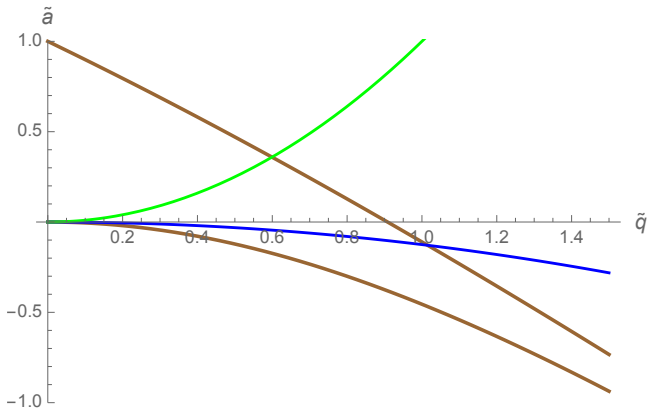

Figure 3.3: Radial analytical curve (green line) $(\tilde{q}_w(q), \tilde{a}_w(q))$ and axial analytical curve (blue line) $(\tilde{q}_z(q), \tilde{a}_z(q))$ inside the Mathieu stability diagram.

and similarly rewrite (3.31) as

$$\ddot{z} + [\tilde{a}_z - 2\tilde{q}_z \cos(2t)]z = 0, \tag{3.34}$$

where

$$\tilde{q}_z = 2q, \quad \tilde{a}_z = -\frac{\tilde{q}_z^2}{8}. \tag{3.35}$$

The results, (3.33) and (3.35), are depicted in Fig. 3.3, which shows the $\tilde{a}(q)$'s and $\tilde{q}(q)$'s plotted in the $a-q$ stability diagram of the Mathieu equation. We see that both the radial and axial curves lie entirely inside of the Mathieu stability region. The radial curve crosses outside of the stability region at $\tilde{q}_w = q = 0.599279 > q_{MI}$, while the axial curve crosses outside of the stability region at $\tilde{q}_z = 1.01612$, which corresponds to $q = 0.508059 > q_{MI}$. Based on the crude assumption of constancy of $x_f(t)$, our results hint towards the fact that the two-ion crystal is stable until the Mathieu instability is reached. Moreover, in agreement with our

numerical results, the crystal loses center-of-mass stability before relative stability. While the results are enlightening, they are not accurate because we know that $x_f(t)$ is not constant.

Taylor Expansion: Therefore, we take into account the oscillatory term in (3.29) to obtain

$$\ddot{w} + \{\frac{q^2}{[1 - \frac{q}{2}\cos(2t)]^3} - 2q\cos(2t)\}w = 0, \tag{3.36}$$

and

$$\ddot{z} + \{\frac{-\frac{q^2}{2}}{[1 - \frac{q}{2}\cos(2t)]^3} + 4q\cos(2t)\}z = 0. \tag{3.37}$$

Expanding the terms in the curly brackets to first order in q, we can write (3.36) in Mathieu's canonical form

$$\ddot{w} + [\bar{a}_w - 2\bar{q}_w\cos(2t)]w = 0, \tag{3.38}$$

where

$$\bar{q}_w = q - \frac{3q^3}{4}, \quad \bar{a}_w = q^2, \tag{3.39}$$

and (3.37) in Mathieu's canonical form as well

$$\ddot{z} + [\bar{a}_z - 2\bar{q}_z\cos(2t)]z = 0, \tag{3.40}$$

where

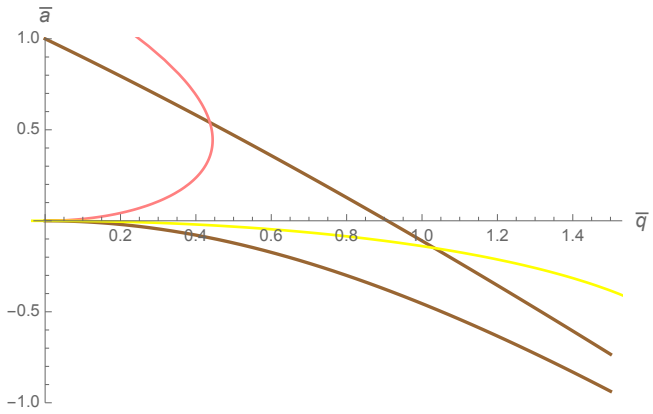

Figure 3.4: Radial analytical curve (pink line) $(\bar{q}_w(q), \bar{a}_w(q))$ and axial analytical curve (yellow line) $(\bar{q}_z(q), \bar{a}_z(q))$ inside the Mathieu stability diagram.

$$\bar{q}_z = 2q - \frac{3q^3}{8}, \quad \bar{a}_z = -\frac{q^2}{2}. \tag{3.41}$$

The results, (3.39) and (3.41), are depicted in Fig. 3.4, which shows the $\bar{a}(q)$'s and $\bar{q}(q)$'s plotted in the $a-q$ stability diagram of the Mathieu equation. Again, we observe that both the radial and axial curves lie entirely inside of the Mathieu stability region. The radial curve crosses outside of the stability region at $\bar{q}_w = 0.437207$, which corresponds to $q = 0.734974 > q_{MI} = 0.454023$, while the axial curve crosses outside of the stability region at $\bar{q}_z = 1.03332$, which corresponds to $q = 0.547417 > q_{MI} = 0.454023$. The results we obtained in this section via first-order Taylor approximation agree with that in the previous section where we assumed $x_f(t)$ to be constant. At this point, we are almost certain that the two-ion crystal is stable until the Mathieu instability is reached. However, Taylor expansion is accurate only if $\frac{q}{2}\cos(2t) \ll 1$, which, depending on the value of q, is not necessarily true.

Fourier Series: Therefore, we expand $x_f(t)$ in a Fourier series, which is exact and accurate up to and including terms that contain $\cos(2t)$. Using the expression for $x_f(t)$ (3.29), we obtain (3.36) and (3.37). Then, we expand the term $\frac{1}{[1-\frac{q}{2}\cos(2t)]^3}$ in a Fourier cosine series up to second order, which gives us

$$\frac{1}{[1-\frac{q}{2}\cos(2t)]^3} = A + B\cos(2t), \tag{3.42}$$

where

$$A = \frac{4(8+q^2)\sqrt{\frac{2+q}{2-q}}}{(-2+q)^2(2+q)^3}, \quad B = \frac{48q\sqrt{\frac{2+q}{2-q}}}{(-2+q)^2(2+q)^3}. \tag{3.43}$$

By inserting (3.42) into (3.36) and (3.37), we then obtain two canonical Mathieu's equations

$$\ddot{w} + [a_w^{(f)} - 2q_w^{(f)}\cos(2t)]w = 0, \tag{3.44}$$

where

$$q_w^{(f)} = q - \frac{Bq^2}{2}, \quad a_w^{(f)} = Aq^2, \tag{3.45}$$

and

$$\ddot{z} + [a_z^{(f)} - 2q_z^{(f)}\cos(2t)]z = 0, \tag{3.46}$$

where

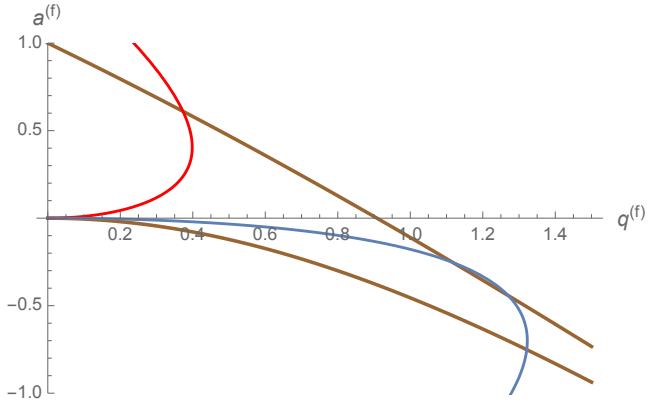

Figure 3.5: Radial analytical curve (red line) $(q_w^{(f)}(q), a_w^{(f)}(q))$ and axial analytical curve (grey line) $(q_z^{(f)}(q), a_z^{(f)}(q))$ inside the Mathieu stability diagram.

$$q_z^{(f)} = 2q - \frac{Bq^2}{4}, \quad a_z^{(f)} = -\frac{Aq^2}{2}. \tag{3.47}$$

(3.45) and (3.47), are illustrated in Fig. 3.5, which shows the $a^{(f)}(q)$'s and $q^{(f)}(q)$'s plotted in the $a-q$ stability diagram of the Mathieu equation. Again, we observe that both the radial and axial curves lie entirely inside of the Mathieu stability region. The radial curve crosses outside of the stability region at $q_w^{(f)} = 0.372837$, which corresponds to $q = 0.659132 > q_{MI} = 0.454023$, while the axial curve first crosses outside of the stability region at $q_z^{(f)} = 1.12036$, which corresponds to $q = 0.6166 > q_{MI} = 0.454023$. The results we obtained in this section via second-order Fourier expansion agree with that in the previous sections, where we Taylor-expanded, and assumed constancy of $x_f(t)$. Moreover, they are close to the numerical results which tells us the crystal loses relative stability at $q = 0.67$ in both the radial and axial directions.

The results are important as we have shown, in two ways, that the relative motion of the two-ion planar crystal is more stable than the center-of-mass motion, and

remains stable beyond the Mathieu instability limit q_{MI}. First, according to (3.45) and (3.47), the effective q's, $q_w^{(f)}$ and $q_z^{(f)}$, are smaller than q. Second, both the radial and axial curves cross the Mathieu stability boundary at q's that are larger than q_{MI}, where the center of mass of the crystal becomes unstable. Therefore, in summary, our analytical results provide strong support for our rigorous semi-analytical proof that the two-ion crystal is stable, without damping, until the Mathieu instability is reached.

3.2 Damped case

Moving on to the damped case, we first need to confirm that the Mathieu instability q_{MI} remains unchanged with $\gamma = 0.001$, the upper bound of damping for which the proposed q_c holds [16–18]. We ran a simulation with $q = 0.454 \approx q_{MI} = 0.454023$ and $\gamma = 0.001$, and found that an ion can be stably trapped. Strobed at the end of each drive cycle, we plotted the Poincare sections of the ion, for the last 200 drive cycles out of 200000, in Fig. 3.6. They indicate that the ion is trapped at the center of the trap.

Now that we have confirmed that the center-of-mass stability is not lost before q_{MI}, we may analyze the relative motion stability of the two-ion crystal. So, we write the damped version of (3.4)

$$\ddot{w} + \gamma\dot{w} + [\frac{2}{x_f^3} - 2q\cos(2t)]w = 0, \tag{3.48}$$

and that of (3.5)

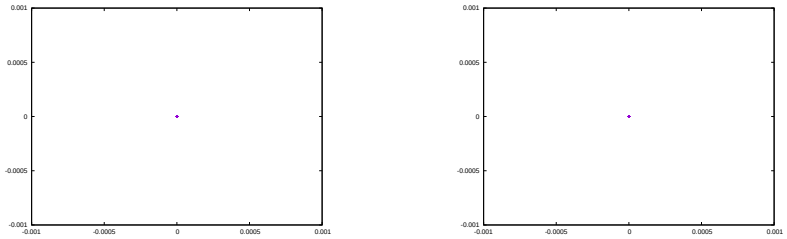

(a) The radial Poincare section $(r, \dot{r})$.

(b) The axial Poincare section $(z, \dot{z})$.

Figure 3.6: The Poincare sections of an ion in a Paul Trap with $q = 0.454$ and $\gamma = 0.001$.

$$\ddot{z} + \gamma\dot{z} + [\frac{-1}{x_f^3} + 4q\cos(2t)]z = 0. \tag{3.49}$$

Since we have introduced the damping terms, the $a-q$ Mathieu stability diagram is not applicable here. However, the absence of the nonlinear Coulomb term suggests that numerical simulations may not be our only choice of approach. As it turns out, we can come up with numerical and analytical methods, similar to those used in Sec. 3.1. The key insight is that by changing the variables, we can turn (3.48) and (3.49) into undamped Mathieu's equations. Then, the machinery of this section will follow that of Sec. 3.1.

First, we consider (3.48) and let

$$\omega = e^{\frac{\gamma t}{2}} w. \tag{3.50}$$

Then, we get

$$\ddot{\omega} + [\alpha_w - 2q\cos(2t)]\omega = 0, \tag{3.51}$$

where

$$\alpha_w = \frac{2}{x_f^3} - \frac{\gamma^2}{4}. \tag{3.52}$$

Now, we turn to (3.49) and let

$$\zeta = e^{\frac{\zeta t}{2}} z. \tag{3.53}$$

Then, we may write

$$\ddot{\zeta} + [\alpha_z + 4q\cos(2t)]\zeta = 0, \tag{3.54}$$

where

$$\alpha_z = \frac{-1}{x_f^3} - \frac{\gamma^2}{4}. \tag{3.55}$$

3.2.1 Semi-analyical Approach

Since both (3.51) and (3.54) are linear, second-order ordinary differential equations with time-periodic coefficients, Floquet theory is applicable [25, 26]. As a result of Floquet theory, we state that the solutions of (3.51) are of the form

$$\omega(t) = e^{i\nu_\omega(q)t}\Omega(t), \tag{3.56}$$

where $\nu_\omega(q)$ is a q-dependent constant and

$$\Omega(t) = \Omega(t+T) \tag{3.57}$$

is a periodic function of period T. Similarly, the solutions of (3.54) are of the form

$$\zeta(t) = e^{i\nu_\zeta(q)t} Z(t), \tag{3.58}$$

where $\nu_\zeta(q)$ is a q-dependent constant and

$$Z(t) = Z(t+T). \tag{3.59}$$

The equations of motion in the new coordinate system (3.48) and 3.49 differ from those in the original coordinate system (3.4) and (3.5) by a constant term $-\frac{\gamma^2}{4}$ in the square bracket. However, they are both second-order linear differential equations for which Floquet Theory holds. Therefore, we adopt the same semi-analytical stability analysis in the undamped case here. For our numerical calculations, we set $\gamma = 0.001$. We then define $\tilde{\mathbf{A}}(q)$ and $\tilde{\mathbf{B}}(q)$ as the mapping matrices for the ω-motion and ζ-motion, respectively. They share the same properties as (3.10). $Tr(\tilde{\mathbf{A}})$ and $Tr(\tilde{\mathbf{B}})$ are depicted as a function of q in (3.7).

The results for the undamped case (see Fig. 3.1) are almost the same as the results here (see Fig. 3.7). At each q, the difference of the points in Figs. 3.1 and 3.7 is at most on the order of 10^{-4}. As expected, $Tr(\tilde{\mathbf{A}}) > 2$ at $q = 0.67 > q_{MI}$ and $Tr(\tilde{\mathbf{B}}) > 2$ at $q = 0.67 > q_{MI}$. Both of the q-values are greater than q_{MI}, which shows that, similar to the undamped case, the crystal only melt at q_{MI}, rather than q_c.

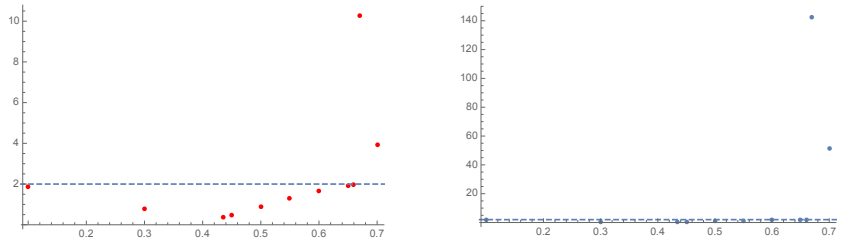

(a) $Tr(\tilde{\mathbf{A}}(q))$ is plotted as a function of q. The dashed lines represents $Tr(\tilde{\mathbf{A}}(q)) = 2$.

(b) $Tr(\tilde{\mathbf{B}}(q))$ is plotted as a function of q. The dashed lines represents $Tr(\tilde{\mathbf{B}}(q)) = 2$.

Figure 3.7: $Tr(\tilde{\mathbf{A}}(q))$ and $Tr(\tilde{\mathbf{B}}(q))$ are plotted as a function of q.

We propose another semi-analytical method that provides a more physical picture. Note that $\nu_\omega(q)$ and $\nu_\zeta(q)$ may be purely real or complex with non-zero imaginary part. We then come up with a stability criterion for w and z, the original variables, as follows:

$$\begin{aligned} w &= e^{-\frac{\gamma t}{2}}\omega(t) \\ &= e^{(i\nu_\omega - \frac{\gamma}{2})t}\varphi(t) \\ &\text{with } \omega(t) = e^{i\nu_\omega t}\varphi(t) \\ &\Rightarrow Re(i\nu_\omega - \frac{\gamma}{2}) \leq 0 \\ &\Rightarrow Re(i\nu_\omega) \leq \frac{\gamma}{2}; \end{aligned} \tag{3.60}$$

$$\begin{aligned} &\text{similarly,} \\ &Re(i\nu_\zeta) \leq \frac{\gamma}{2}. \end{aligned} \tag{3.61}$$

Therefore, if $\nu_\omega(q)$ (or $\nu_\zeta(q)$) is real, the two-ion planar crystal will be stable. If $\nu_\omega(q)$ (or $\nu_\zeta(q)$) is complex with a positive real part, the crystal will be stable. If $\nu_\omega(q)$ (or $\nu_\zeta(q)$) is complex with a negative real part, the crystal will be stable only

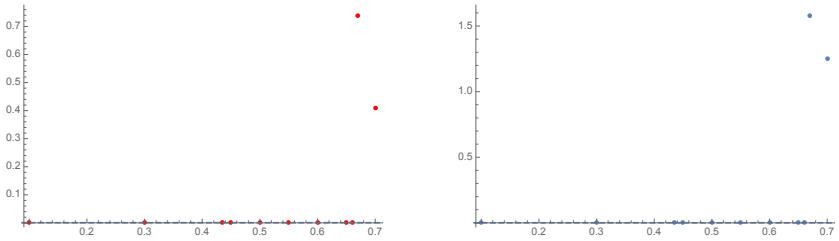

(a) $\nu_\omega(q)$ is plotted as a function of q. The dashed lines represents $\nu_\omega(q) = \frac{\gamma}{2} = 5 \times 10^{-4}$.

(b) $\nu_\zeta(q)$ is plotted as a function of q. The dashed lines represents $\nu_\zeta(q) = \frac{\gamma}{2} = 5 \times 10^{-4}$.

Figure 3.8: $\nu_\omega(q)$ and $\nu_\zeta(q)$ are plotted as a function of q.

if the (3.61) is satisfied. The physical picture is clearly the tug of war between the growing term in the solution and the damping. When the growth of the solution overcomes the suppression from the damping, the relative motion of the two ions turns unstable. $\nu_\omega(q)$ and $\nu_\zeta(q)$ responsible for exponential growth are obtained numerically and illustrated in Fig. 3.8.

We glean from Fig. 3.8 that $\nu_\omega(q) > \frac{\gamma}{2}$ at $q = 0.67 > q_{MI}$ and $\nu_\zeta(q) > \frac{\gamma}{2}$ at $q = 0.67 > q_{MI}$, which agrees with the results from the previous method.

3.2.2 Analytical Approach

The stability analysis in Sec. 3.2.1 is rigorous, only under the assumption that the numerical computations were executed properly. Thus, in this section, we present analytical approximations that support the results presented in Sec. 3.2.1. Same as Sec. 3.1.2, this section is based on the pseudopotential method. By (i) assuming $x_f(t)$ to be constant, and expanding $x_f(t)$ via (ii) Taylor and (iii) Fourier series, we obtain effective (q, a)'s which can be plotted onto the stability diagram. We expect that the effective q's will remain the same as the undamped case because while

the effective a's will be altered by damping because it is constant, rather than periodic. Furthermore, based on the numerical results, we foresee the analytics will show that damping will not affect the crystal's relative-motion stability. For the following analytics, we set $\gamma = 0.001$ for the same reason mentioned in the last paragraph of Sec. 3.2.1.

Assume constant $x_f(t)$: Ignoring the oscillatory term, we assume $x_f(t) = \tilde{x}_f$. Then, we insert (3.28) into (3.51) and (3.54) to obtain

$$\ddot{\omega} + [\tilde{a} - 2\tilde{q}\cos(2t)]\omega = 0, \tag{3.62}$$

where

$$\tilde{a} = q^2 - \frac{\gamma^2}{4}, \quad \tilde{q} = q, \tag{3.63}$$

and

$$\ddot{\zeta} + [\tilde{a} - 2\tilde{q}\cos(2t)]\zeta = 0, \tag{3.64}$$

where

$$\tilde{q} = 2q, \quad \tilde{a} = -\frac{\tilde{q}^2}{8} - \frac{\gamma^2}{4}. \tag{3.65}$$

As expected, only the $\tilde{a}$'s are different from those in the undamped case, while the $\tilde{q}$'s remain unchanged. The analytical curves illustrated in Fig. 3.9 are basically the same as those in (3.3) because they are only dragged down by $\frac{\gamma^2}{4} = 2.5 \times 10^{-7}$. Moreover, the intersection point of the radial curve (or the axial curve) and the

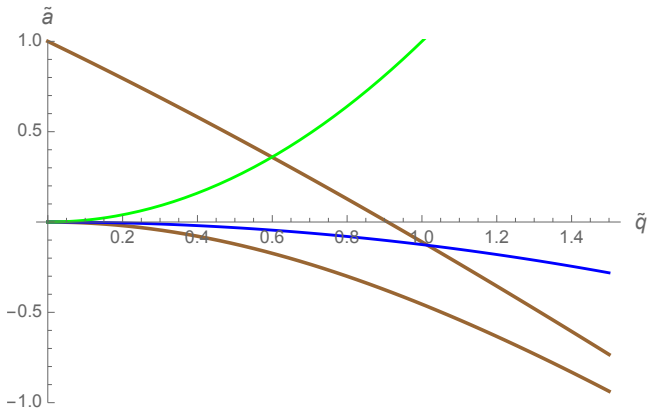

Figure 3.9: Radial analytical curve (green line) $(\tilde{q}_\omega(q), \tilde{a}_\omega(q))$ and axial analytical curve (blue line) $(\tilde{q}_\zeta(q), \tilde{a}_\zeta(q))$ inside the Mathieu stability diagram.

Mathieu boundary is almost indiscernible from that in the undamped case. As a result, the corresponding q values at which the crystal loses radial and axial stability here are larger than those in the undamped case by 1.0721×10^{-7} and 2.62556×10^{-7}. Therefore, the results allude to the fact that $\gamma = 0.001$ increases the relative stability, but only by a very tiny bit.

Taylor Expansion: Here, we take into account of the oscillatory term in (3.29) to obtain

$$\ddot{\omega} + [\bar{a}_\omega - 2\bar{q}_\omega \cos(2t)]\omega = 0, \tag{3.66}$$

where

$$\bar{q}_\omega = q - \frac{3q^3}{4}, \quad \bar{a}_\omega = q^2 - \frac{\gamma^2}{4}, \tag{3.67}$$

and

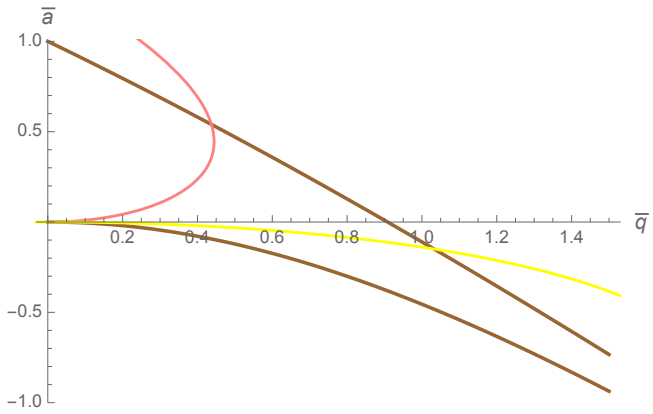

Figure 3.10: Radial analytical curve (pink line) $(\bar{q}_\omega(q), \bar{a}_\omega(q))$ and axial analytical curve (yellow line) $(\bar{q}_\zeta(q), \bar{a}_\zeta(q))$ inside the Mathieu stability diagram.

$$\ddot{\zeta} + [\bar{a}_\zeta - 2\bar{q}_\zeta \cos(2t)]\zeta = 0, \tag{3.68}$$

where

$$\bar{q}_\zeta = 2q - \frac{3q^3}{8}, \quad \bar{a}_\zeta = -\frac{q^2}{2} - \frac{\gamma^2}{4}, \tag{3.69}$$

Again, the analytical curves depicted in Fig. 3.10 are effectively the same as those in Fig. 3.4 because of the damping term. Consequently, the corresponding q values at which the crystal loses radial and axial stability here are larger than those in the undamped case by 2.02778×10^{-7} and 1.70913×10^{-7}. Thus, the results hint at the fact that the damping term increases the relative stability ever so slightly.

Fourier Series: Finally, we expand $x_f(t)$ in a Fourier series to obtain two canonical Mathieu's equations

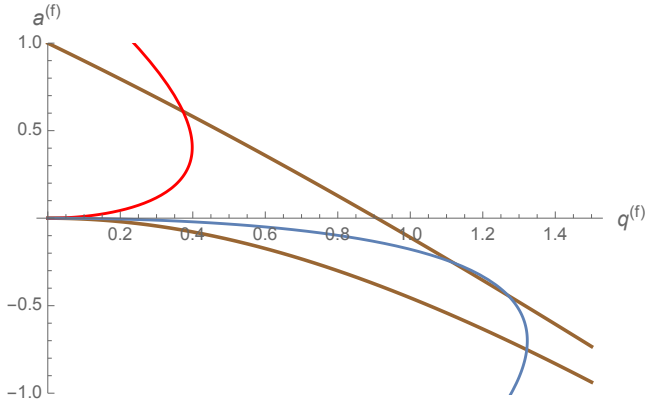

Figure 3.11: Radial analytical curve (red line) $(q_\omega^{(f)}(q), a_\omega^{(f)}(q))$ and axial analytical curve (grey line) $(q_\zeta^{(f)}(q), a_\zeta^{(f)}(q))$ inside the Mathieu stability diagram.

$$\ddot{\omega} + [a_\omega^{(f)} - 2q_\omega^{(f)} \cos(2t)]\omega = 0, \tag{3.70}$$

where

$$q_\omega^{(f)} = q - \frac{Bq^2}{2}, \quad a_\omega^{(f)} = Aq^2 - \frac{\gamma^2}{4}, \tag{3.71}$$

and

$$\ddot{\zeta} + [a_\zeta^{(f)} - 2q_\zeta^{(f)} \cos(2t)]\zeta = 0, \tag{3.72}$$

where

$$q_\zeta^{(f)} = 2q - \frac{Bq^2}{4}, \quad a_\zeta^{(f)} = -\frac{Aq^2}{2} - \frac{\gamma^2}{4}. \tag{3.73}$$

Unsurprisingly, the analytical curves plotted in Fig. 3.11 are essentially the same as those in Fig. 3.5 due to the effect of damping. Resultingly, the corresponding

q values at which the crystal loses radial and axial stability here are larger than those in the undamped case by 1.31888×10^{-7} and 4.38029×10^{-7}, respectively. Therefore, we conclude that $\gamma = 0.001$ does increase the relative stability, albeit by a very tiny margin.

Chapter 4

Dicussions

We rigorously proved that with the ideal Paul trap, in the presence of damping, modeled as $-\gamma\dot{x}$, the so-called "critical" transition does not exist. In hindsight, the following question naturally arises: With respected scientists on both sides of the controversy, how did one side make the error that they did? We approach this question twofold by exploring (i) the numerics in Sec. 4.1.1 and (ii) experimental possible sources of error in Sec. 4.1.2.

4.1 Possible Sources of the Controversy

4.1.1 Numerical Sources

We inspected both sides' numerical simulations and noticed that the noise model and its implementation might be a possible source of error.

First, we consider the noise models adopted by the Munich group and the Beijing group. The Munich group simulated the Paul trap with laser cooling force and

spontaneous emission noise in 1988 [13]; in 1989, they simulated both without noise, and with spontaneous emission noise and the effect of contact potentials [9]. Independent from the Munich group, the Beijing group did not impose noise in their simulation in 1997 [21]. In all their simulations, they did not find the claimed critical transition.

On the other hand, the IBM group ran their simulations without noise and with laser cooling force in 1988 [14]; in their 1990 Nature paper, they simulated without noise [12]. In both papers, their numerical results pointed to the existence of the "critical" transition. Finally, in their review paper, they simulated with "a small noise term applied to q" to simulate the effect of multipoles caused by trap imperfections [16]. However, they did not describe the model they used to simulate this "small noise term", which causes reproducibility issues. Moreover, in Sec. 4.1.2, we will show that the effect of multipoles is highly nonlinear and could be quite large [33, 34]. Therefore, even though they could always reproduce the "critical" transition, the results could be due to an unrealistic noise model.

Yet, that does not explain why contradicting results were produced when both sides simulated without noise, and with laser cooling force. Here we propose that this may be due to the fact that the two sides used different numerical integration methods. Both the Munich and the Beijing groups used the fourth-order Runge-Kutta method, while the IBM group used the Bulirsch-Stoer method. However, both methods are commonly used numerical integration methods. Therefore, that should not matter.

4.1.2 Experimental Sources

We now investigate the possible causes of the melting phenomena observed by the IBM group. We suggest that the possible causes include (i) background gas pressure, (ii) adiabaticity of the experiments, and (iii) trap defects.

It is not likely that the background gas pressure caused the melting of crystals because the IBM group had a lower pressure (6.7×10^{-11}mbar) [15] than the Munich group (2×10^{-10}mbar) [9], and yet the Munich group did not observe the melting of crystals. However, this can be easily verified using state-of-the-art setup which can reach 10^{-15}mbar [35].

The IBM group claimed in [15] the Munich group did not observe the "critical" transition because in their experiments, they were "sweeping the rf voltage rapidly". However, the Munich group clearly stated that they increased q adiabatically in [9].

Last but not least, trap defects and different trap designs create multipoles in the ion traps [36, 37]. The effect of these multipoles is highly nonlinear and extremely difficult to obtain analytically. As an example, we discuss the case of the Paul trap with an added octupole field. The potential in such a trap can be represented by [33, 34]

$$\Phi = \Phi_0[A(\frac{r^2 - 2z^2}{2r_0^2}) + B(\frac{3r^4 - 24r^2z^2 + 8z^4}{8r_0^4})], \tag{4.1}$$

where Φ_0 is the same as that in (2.6), $r = \sqrt{x^2 + y^2}$, and A and B are constants representing the quadrupole and octupole strength, respectively. For simplicity, we consider the motion of one charged particle along the x-axis ($z = 0$). So, the nonlinear effect of $r - z$ coupling term, $-24r^2z^2$, can be avoided. Then, the

equation of motion of a single particle in the x-direction is given by [33]

$$\frac{d^2x}{d\tau^2} + [a - 2q\cos(2\tau)](x + \epsilon\frac{3x^3}{2r_0^2}) = 0, \tag{4.2}$$

where

$$\begin{aligned} a &= \frac{4AQU_0}{m\Omega^2 r_0^2}, \quad q = \frac{2AQV_0}{m\Omega^2 r_0^2}, \\ \tau &= \frac{\Omega t}{2}, \qquad\quad \epsilon = \frac{B}{A}. \end{aligned} \tag{4.3}$$

The constants $Q, U_0, V_0, m, \Omega, r_0$ follow from the notations in Sec. 2. Equation (4.3) is a *nonlinear Mathieu Equation*, where ϵ is a dimensionless constant representing the ratio between the octupole and quadrupole strength. In the single-particle case, we can already see from the cubic term, $\frac{3r^3}{2r_0^2}$, that the particle's radial distance from the trap center, r, can lead to trajectories that drift further away from the trap center, and hence, instability. Therefore, the stability of the particle depends on the octupole and damping (if added) strengths. If we consider the two-particle case, the addition of the nonlinear Coulomb force will further complicate the analysis. Therefore, multiple-particle cases await further investigation, which is beyond the scope of this thesis.

Chapter 5

Outlook

5.1 Implications of the Results

In addition to the fact that this thesis resolves the controversy, the method we developed can be extended to solve other problems. First, we can use it to analytically trace the crystal-free regions in the Mathieu stability diagram, where ions have center-of-mass stability, but not relative stability [10]. That is because even with non-zero a's, we can linearize the equations of relative motion and then, analytically find the (q, a)'s that lead to instability. Second, since the equations of motion of charged particles in a hyperbolic Paul trap are almost identical to that in a linear Paul trap, we can use the method to show that two-ion crystals are stable at high q's in a linear Paul trap. Now, a higher q leads to a stronger restoring force, which then lead to a higher transversal phonon mode frequency of the two ions. This in turn leads to a higher bus speed in ion trap quantum computers [38].

Appendix A

Solving Mathieu's Equation

Mathieu's equation is a second-order, linear differential equation and has the canonical form [25]

$$\frac{d^2u}{dt^2} + [a - 2q\cos(2t)]u = 0. \tag{A.1}$$

First, we notice that a Mathieu's equation is parametrized by q and a. Therefore, the points in the (q, a) two-dimensional parameter space determine the type of solutions to the equation. Here, we consider the case where both q and a are real numbers because in the Paul Trap system, they embody physical control parameters, i.e., ac and dc voltages, that can be experimentally tuned. Also, we can restrict q to be positive without affecting the general solution to (A.1) as a sign change of the q-term in (A.1) can be accomplished by a change in the zero-point of t.

The key feature of (A.1) that helps us arrive at the general solution is the periodic driving term. It allows us to apply Floquet theory [25, 26], a theorem in the theory

of ordinary differential equations relating to the class of solutions to periodic linear differential equations of the form

$$\dot{\vec{x}} = \mathbf{A}(t)\vec{x}, \tag{A.2}$$

with $\mathbf{A}(t)$ a periodic function. Here, $\mathbf{A}(t)$ is represented in a matrix

$$\mathbf{A}(t) = \begin{pmatrix} 0 & 1 \\ 2q\cos(2t) - a & 0 \end{pmatrix} \tag{A.3}$$

and $\vec{x}$ is given by

$$\vec{x}(t) = \begin{pmatrix} u(t) \\ \dot{u}(t) \end{pmatrix}. \tag{A.4}$$

According to Floquet theory [26], there then exists a Floquet solution to (A.1) that assumes the form

$$u_1(t) = e^{i\mu t}U(t), \tag{A.5}$$

where $\mu = a+ib$ may be complex where a, b are real numbers and $U(t)$ is a periodic function with the same period as $\mathbf{A}$, which is π. Therefore, $U(t)$ is bounded and the *Floquet exponent* μ of the term $e^{i\mu t}$ solely determines the stability of the solution. While Floquet Theory does give us one solution, we still need a second solution, linearly independent from the first, to arrive at a general solution. Thus, we shall construct the general solutions, based on three different categories of μ, and determine their stability.

(1) Consider the case in which $b \neq 0$ and μ is complex. Then, the general solution to (A.1) assumes the form [25]

$$u(t) = Ae^{i\mu t}U(t) + Be^{-i\mu t}U(-t) \tag{A.6}$$

with A and B constants of integration. Due to the fact that b is non-zero, as t goes to infinity, one of the two terms on the right of (A.6) must go to infinity as well, and the other term goes to zero. Therefore, the general solution $u(t)$ is unstable when μ is complex.

(2) Consider the case in which $b = 0$ and μ is an integer. Then, since $U(t)$ has period π, the Floquet solution $u_1(t)$ has period π if μ is even, and 2π if μ is odd. Here, we cannot obtain the general solution merely by adding $u_1(-t)$ because they are not linearly independent from each other. Instead, the second solution is given by [25]

$$u_2(t) = Ctu_1(t) + g(t), \tag{A.7}$$

where C is a constant, and $g(t)$ has the same period as $u_1(t)$. We can immediately tell that $u_2(t)$ is unstable because as t goes to infinity, the first term on the right of (A.7) goes to infinity. In conclusion, if μ is an integer, the general solution will be unstable.

(3) Now comes the third and last case in which $b = 0$ and μ is real, but not an integer. Then, $u_1(t)$ and $u_2(t)$ are linearly independent solutions [25]. Moreover, since $b = 0$, the general solution is stable. Given the special case where μ is a rational number, say $\mu = \frac{m_1}{m_2}$, then the general solution will be of period at most $2m_2\pi$.

Note that the definition of μ might be a bit ambiguous because part of the exponential term $e^{i\mu t}$ can be absorbed into $U(t)$ in the following manner:

First, define

$$\mu = \mu_k + 2k, \tag{A.8}$$

with k an arbitrary integer and μ_k denoted as the *(Mathieu) characteristic exponent*, and

$$\tilde{U}(t) = e^{2ikt}U(t), \tag{A.9}$$

where $\tilde{U}(t)$ has the same period as $U(t)$ and hence, $\mathbf{A}$. Then, A.5 becomes the following:

$$u_1(t) = e^{i\mu t}U(t) = e^{i(\mu_k+2k)t}U(t) = e^{i\mu_k t}\tilde{U}(t), \tag{A.10}$$

and $u_1(t)'s$ Floquet form is retained.

Therefore, if μ is an even integer, then we set $2k = \mu$ and the characteristic exponent μ_k will be zero; if μ is an odd integer, then we set $2k = \mu - 1$ and μ_k will be 1. In the even case, the solution is π-periodic, and in the odd case, the solution is 2π-periodic.

Appendix B

Pseudopotential

The pseudopotential method is the mathematical theory of dynamical stabilization of an unstable equilibrium point first published by Kapitza [39]. The method will be derived in one dimension, but is easily generalized to higher dimensions.

First, we consider a particle of mass m perturbed by a force

$$F(x,t) = f(x)\cos(\omega t), \tag{B.1}$$

where $f(x)$ is the form factor of the force F. Under the force F, the particle's trajectory is described by $x(t)$. We define the local time average of a function $f(t)$ according to

$$\langle f(t)\rangle = \frac{1}{T}\int_0^T f(t+t')dt', \tag{B.2}$$

where T is the period. We now let $T = \frac{2\pi}{\omega}$. Using our definition (B.2), we reach the key insight of the pseudopotential method: the motion $x(t)$ may be split into

a slow, guiding-center macro-motion $X(t)$, and a fast vibrating micro-motion $\xi(t)$. Then, we may write

$$x(t) = X(t) + \xi(t). \tag{B.3}$$

Furthermore, the method assumes

$$\langle X(t) \rangle \approx X(t), \quad \langle \xi(t) \rangle = 0; \tag{B.4}$$

and

$$|X(t)| \gg |\xi(t)|, \quad |\ddot{X}(t)| \ll |\ddot{\xi}(t)|. \tag{B.5}$$

Based on these assumptions, we can expand the equation of motion for the particle as follows:

$$\begin{aligned} m\ddot{x}(t) &= m\ddot{X}(t) + m\ddot{\xi}(t) \\ &= f(x(t)) \cos(\omega t) \\ &= f(X(t)) \cos(\omega t) + \xi(t) \cos(\omega t) \frac{\partial f}{\partial X}. \end{aligned} \tag{B.6}$$

We now equate the fast terms in (B.6) to get

$$\begin{aligned} &m\ddot{\xi}(t) = f(X(t)) \cos(\omega t), \\ &\text{which is then integrated to obtain} \\ &\xi(t) = -\frac{f(X)}{mw^2} \cos(\omega t). \end{aligned} \tag{B.7}$$

Using (B.7), the local time average of (B.6) yields

$$\begin{aligned} m\ddot{X}(t) &= \langle \xi(t)\cos(\omega t)\frac{\partial f}{\partial X}\rangle \\ &= -\frac{1}{2m\omega^2} f(X)\frac{\partial f(X)}{\partial X}. \end{aligned} \tag{B.8}$$

We then rewrite (B.8) as

$$m\ddot{X} = -\frac{\partial U_{eff}(X)}{\partial X}, \tag{B.9}$$

where

$$U_{eff}(X) = \frac{1}{4m\omega^2} f^2(X) \tag{B.10}$$

is the effective potential, or the *pseudopotential*.

Appendix C

Linearizing the Two-Particle Equations of Relative Motion

The perturbed equations of relative motion for a undamped two-ion crystal at $a = 0$ are given by (3.3). We first linearize the radial part of (3.3) through Taylor expansion and by keeping only linear order perturbation terms.

$$\begin{aligned} \ddot{x_f} + \ddot{w} - [2q\cos(2t)](x_f + w) &= \frac{x_f + w}{[(x_f + w)^2 + z^2]^{\frac{3}{2}}} \\ &= \frac{x_f + w}{[x_f^2 + 2x_f w]^{\frac{3}{2}}} \\ &= \frac{x_f + w}{x_f^3[1 + \frac{2w}{x_f}]^{\frac{3}{2}}} \\ &= \frac{x_f + w}{x_f^3}[1 - \frac{3w}{x_f}] \\ &= \frac{1}{x_f^2} - \frac{2w}{x_f^3}. \end{aligned} \tag{C.1}$$

By recognizing that x_f is a solution to the radial part of (3.1), we get

$$\ddot{x_f} - 2q\cos(2t)x_f = \frac{1}{x_f^2}, \tag{C.2}$$

which uses the fact that $x_f > 0$ for all t. Then, we can further simplify (C.1) into

$$\ddot{w} + [\frac{2}{x_f^3} - 2q\cos(2t)]w = 0, \tag{C.3}$$

which is the linearized radial part of (3.3).

We then linearize the axial part of (3.3).

$$\begin{aligned} \ddot{z} + [4q\cos(2t)]z &= \frac{z}{[(x_f + w)^2 + z^2](\frac{3}{2})} \\ &= \frac{z}{[x_f + w]^3} \\ &= \frac{z}{x_f^3[1 + \frac{w}{x_f}]^3} \\ &= \frac{z}{x_f^3}[1 - \frac{3w}{x_f}] \\ &= \frac{z}{x_f^3}. \end{aligned} \tag{C.4}$$

Then, we simplify (C.4) into

$$\ddot{z} + [\frac{-1}{x_f^3} + 4q\cos(2t)]z = 0, \tag{C.5}$$

which is the linearized axial part of (3.3).

For the damped case, we may just add in the damping terms and obtain

$$\ddot{w} + \gamma\dot{w} + [\frac{2}{x_f^3} - 2q\cos(2t)]w = 0 \tag{C.6}$$

for the radial part, and

$$\ddot{z} + \gamma\dot{z} + [\frac{-1}{x_f^3} + 4q\cos(2t)]z = 0, \tag{C.7}$$

for the axial part because linearization does not alter the damping term.

Bibliography

[1] Wolfgang Paul, "Electromagnetic traps for charged and neutral particles," Rev. Mod. Phys. **62**, 531–540 (1990).

[2] R. Blümel, "Nonlinear dynamics of trapped ions," Physica Scripta T **59**, 369–379 (1995).

[3] J. Zhang, P. W. Hess, A. Kyprianidis, P. Becker, A. Lee, J. Smith, G. Pagano, I.-D. Potirniche, A. C. Potter, A. Vishwanath, N. Y. Yao, and C. Monroe, "Observation of a discrete time crystal," Nature **543**, 217?220 (2017).

[4] J. I. Cirac and P. Zoller, "Quantum computations with cold trapped ions," Phys. Rev. Lett. **74**, 4091–4094 (1995).

[5] Raymond E. March, "An introduction to quadrupole ion trap mass spectrometry," Journal of mass spectrometry **32**, 351–369 (1997).

[6] Bruno Domon and Ruedi Aebersold, "Mass spectrometry and protein analysis," Science **312**, 212–217 (2006).

[7] Weihua Guan, Sony Joseph, Jae Hyun Park, Predrag S. Krstić, and Mark A. Reed, "Paul trapping of charged particles in aqueous solution," Proceedings of the National Academy of Sciences **108**, 9326?9330 (2011).

[8] Sony Joseph, Weihua Guan, Mark A. Reed, and Predrag S. Krstić, "A long

dna segment in a linear nanoscale paul trap," Nanotechnology **21**, 015103 (2009).

[9] R. Blümel, C. Kappler, W. Quint, and H. Walther, "Chaos and order of laser-cooled ions in a paul trap," Phys. Rev. A **40**, 808–823 (1989).

[10] J. W. Emmert, M. Moore, and R. Blümel, "Prediction of a deterministic melting transition of two-ion crystals in a paul trap," Phys. Rev. A **48**, R1757–R1760 (1993).

[11] R. Blümel, "Cooling-induced melting of ion crystals in a paul trap," Phys. Rev. A **51**, 620–624 (1995).

[12] R. G. Brewer, J. Hoffnagle, R. G. DeVoe, L. Reyna, and W. Henshaw, "Collision-induced two-ion chaos," Nature (London) **344**, 305–309 (1990).

[13] R. Blümel, J. M. Chen, E. Peik, W. Quint, W. Schleich, Y. R. Shen, and H. Walther, "Phase transitions of stored laser-cooled ions," Nature (London) **334**, 309–313 (1988).

[14] J. Hoffnagle, R.G. DeVoe, L. Reyna, and R.G. Brewer, "Order-chaos transition of two trapped ions," Phys. Rev. Lett. **61**, 255–258 (1988).

[15] R.G. Brewer, J. Hoffnagle, and R.G. DeVoe, "Transient two-ion chaos," Phys. Rev. Lett. **65**, 2619–2622 (1990).

[16] J. Hoffnagle and R.G. Brewer, "Chaotic transients of two particles in a paul trap: Interpretation as a boundary crisis," Phys. Rev. A **50**, 4157–4169 (1994).

[17] J. A. Hoffnagle and R.G. Brewer, "Two-ion chaos," Physica Scripta T **59**, 380–386 (1995).

[18] Raymond Y. Chiao, ed., *Amazing Light: A Volume Dedicated to Charles Hard Townes On His 80th Birthday* (Springer-Verlag, New York, 1996).

[19] J. Hoffnagle and R. G. Brewer, "On the frequency-locked orbits of two particles in a paul trap," Science **265**, 213–215 (1994).

[20] J. Hoffnagle and R.G. Brewer, "Frequency-locked motion of two particles in a paul trap," Phys. Rev. Lett. **71**, 1828–1831 (1993).

[21] Jing-Ling Shen, Hua-Wei Yin, Jian-Hua Dai, and Hong-Jun Zhang, "Dynamical behavior, transient chaos, and riddled basins of two charged particles in a paul trap," Phys. Rev. A **55**, 2159–2164 (1997).

[22] F. G. Major, V. N. Gheorghe, and G. Werth, *Charged Particle Traps: Physics and Techniques of Charged Particle Field Confinement* (Springer-Verlag, Berlin Heidelberg, 2005).

[23] David J. Griffiths, *Introduction to Electrodynamics* (Pearson, 2013).

[24] D. K. Weiss, *Wesleyan University summer research poster* (2015).

[25] M. Abramowitz and I. A. Stegun, eds., *Handbook of Mathematical Functions* (National Bureau of Standards, Gaithersburg, MD, 1964).

[26] G. Floquet, "Sur les quations diffrentielles linaires coefficients priodiques," Annales scientifiques de l'cole normale suprieure **12**, 47–88 (1883).

[27] R. Blümel, "Nonlinear dynamics of trapped ions," Physica Scripta T **59**, 434–437 (1995).

[28] A. M. Lyapunov, "The general problem of the stability of motion," International Journal of Control **55**, 531–534 (1992).

[29] Edward Ott, *Chaos in Dynamical Systems* (Cambridge University Press, 2002).

[30] M. G. Moore and R. Blümel, "An improved pseudo potential for the two-ion paul trap," Physica Scripta T **59**, 429–433 (1995).

[31] D. J. Wineland, J. C. Bergquist, Wayne M. Itano, J. J. Bollinger, and C. H. Manney, "Atomic-ion coulomb clusters in an ion trap," Phys. Rev. Lett. **59**, 2935–2938 (1987).

[32] M. Drewsen, C. Brodersen, L. Hornekær, J. S. Hangst, and J. P. Schifffer, "Large ion crystals in a linear paul trap," Phys. Rev. Lett. **81**, 2878–2881 (1998).

[33] et al. Xiong, Caiqiao, "A theoretical method for characterizing nonlinear effects in paul traps with added octopole field," Journal of The American Society for Mass Spectrometry **26**, 1338–1348 (2015).

[34] et al. Xiong, Caiqiao, "Nonlinear ion harmonics in the paul trap with added octopole field: Theoretical characterization and new insight into nonlinear resonance effect," Journal of The American Society for Mass Spectrometry **27**, 344–351 (2016).

[35] et al. Brandl, M. F., "Cryogenic setup for trapped ion quantum computing," Review of Scientific Instruments **87**, 113103 (2016).

[36] Earl C. Beaty, "Calculated electrostatic properties of ion traps," Phys. Rev. A **33**, 3645–3656 (1986).

[37] Gerald Gabrielse, "Relaxation calculation of the electrostatic properties of compensated penning traps with hyperbolic electrodes," Phys. Rev. A **27**, 2277–2290 (1983).

[38] Chris Monroe Zhu, Shi-Liang and L-M. Duan, "Trapped ion quantum computation with transverse phonon modes," Phys. Rev. Lett. **97**, 050505 (2006).

[39] P. L. Kapitza, "Dynamic stability of a pendulum with an oscillating point of suspension," Zh. Eksperim. i. Teor. Fiz. **21**, 588 (1951).